QUANTUM FLUCTUATION EFFECTS ON NUCLEAR MULTIFRAGMENTATION

Akira Ohnishi
Division of Physics, Graduate School of Science,
Hokkaido University, Sapporo 060, Japan

Jørgen Randrup
Nuclear Science Division, Lawrence Berkeley National Laboratory,
Berkeley, CA 94720, USA

The effects of quantum fluctuations are studied by using the recently developed Quantal Langevin model. It is shown that we can understand various thermal and dynamical aspects of nuclear matter, such as the caloric curve, fragment mass distribution in a thermal environment, and abundant IMF productions in Au+Au collisions in a consistent and microscopic way by taking account of the inherent energy fluctuations within the wave packet wave functions.

1 Introduction

Multifragmentation may be caused by the instability of nuclear matter in the spinodal region, in which nuclear liquid and gas phase co-exist. This idea has recently received renewal interest, after the extraction of a caloric curve of hot nuclear matter [1] suggesting that the phase transition is of first-order. It is a big challenge for theoretists to elucidate the relation between the fragment formation in the final state and this liquid-gas phase transition, which is expected to occur dynamically during the heavy-ion collision. For this purpose, we have to invoke models which take due account of the quantum statistical nature of the nuclear system at equilibrium, since the nuclear liquid phase may be characterized by its quantal statistical nature, $E^* \propto T^2$.

In statistical models, the quantum statistical nature of nuclear system is realized by considering the mixture of nucleons and fragments, and the empirical level densities of fragments. The initial condition to these models, such as the excitation energy, charge and mass of the equilibrated system, are usually given by dynamical transport models or considered to be free parameters to fit the data. However, the possible importance of the quantal statistical nature in the pre-equilibrium stage cannot be addressed in these approaches. On the other hand, the applicability of semi-classical transport models, such as the Quantum Molecular Dynamics (QMD), to these phenomena can be problematic, since their statistical properties are essentially classical.

To take approximate account of the quantal statistical features of the

evolving nuclear system, we incorporate a stochastic term given by the recently developed *Quantal Langevin* model [2] into wave packet dynamics. The Quantal Langevin model has been constructed based on the requirement that the system evolves to relax towards quantum-statistical equilibrium by taking account of the inherent energy fluctuations within the wave packet wave functions. Then it is expected to improve the description of fragment formation processes, where the quantum statistics plays an important role.

In this report, we present the basic idea of the Quantal Langevin model and show that various thermal and dynamical aspects of nuclear matter, such as the caloric curve, fragment mass distribution in a thermal environment, and abundant IMF productions in Au+Au collisions, can be understood in a consistent and microscopic way.

2 Nuclear Caloric Curve — Statistical Properties of Nuclei

The starting point of our discussion is the description of quantal statistical nature of nuclear system at equilibrium, by using wave packet basis states, which we are treating in microscopic transport models. Statistical properties are governed by the partition function,

$$\mathcal{Z}(\beta) \equiv \mathrm{Tr}\left(e^{-\beta\hat{H}}\right) = \int d\Gamma\, \mathcal{W}_\beta(\boldsymbol{Z}) \ , \quad \mathcal{W}_\beta(\boldsymbol{Z}) \equiv \langle \boldsymbol{Z}|\, e^{-\beta\hat{H}}\, |\boldsymbol{Z}\rangle \ , \qquad (1)$$

where $|\boldsymbol{Z}\rangle$ represents a parametrized and normalized wave packet wave function, and $\int d\Gamma\, |\boldsymbol{Z}\rangle\langle\boldsymbol{Z}|$ resolves unity. When the basis states $|\boldsymbol{Z}\rangle$ is an energy eigen state, the statistical weight $\mathcal{W}_\beta(\boldsymbol{Z})$ reduces to a usual Boltzmann factor, $\exp(-\beta\mathcal{H})$, with the energy expectation value $\mathcal{H} \equiv \langle \boldsymbol{Z}|\hat{H}|\boldsymbol{Z}\rangle$. However, wave packet wave functions are not energy eigen states, but have finite energy dispersions, $\sigma_{_E}^2(\boldsymbol{Z}) \equiv \langle \boldsymbol{Z}|\hat{H}^2 - \mathcal{H}^2|\boldsymbol{Z}\rangle \neq 0$. At high temperatures, this statistical weight can be expanded in β, $\log \mathcal{W}_\beta(\boldsymbol{Z}) = -\beta\mathcal{H}(\boldsymbol{Z}) + \beta^2\sigma_{_E}^2(\boldsymbol{Z})/2 + \mathcal{O}(\beta^3)$. The classical statistical weight of a wave packet $e^{-\beta\mathcal{H}}$ is then only valid when the temperature is high enough compared to the effective energy scale, $D(\boldsymbol{Z}) = \sigma_{_E}^2/\mathcal{H}$. At lower temperatures, therefore, the energy dispersion of each wave packet is equally or more important compared to the enery expectation value in a quantum statistical context.

In addition to the above modification of the statistical weight, the *intrinsic distortion* effect of wave packets is also important in evaluating observables in quantum statistics. The definition of the thermal average of an operator reads,

$$\prec \hat{O} \succ_\beta = \frac{1}{\mathcal{Z}_\beta} \int d\Gamma\, \mathcal{W}_\beta(\boldsymbol{Z})\ \mathcal{O}_\beta(\boldsymbol{Z}) \ , \quad \mathcal{O}_\beta(\boldsymbol{Z}) = \frac{\langle \boldsymbol{Z}_{\beta/2}|\hat{O}|\boldsymbol{Z}_{\beta/2}\rangle}{\langle \boldsymbol{Z}_{\beta/2}|\boldsymbol{Z}_{\beta/2}\rangle} \ . \qquad (2)$$

These relations show that the thermal mean value is the weighted average of the expectation value with the distorted wave packet $|\boldsymbol{Z}_{\beta/2}\rangle = \exp(-\beta\hat{H}/2)|\boldsymbol{Z}\rangle$, not with the wave packet $|\boldsymbol{Z}\rangle$ itself. This is because the canonical weight operator $\exp(-\beta\hat{H})$ modifies the relative weight of energy eigen components within a wave packet.

As a tractable and reliable way to include the above energy dispersion effects within a wave packet, we have proposed the *harmonic approximation* to this statistical weight [2,3],

$$\mathcal{W}(\boldsymbol{Z}) \approx \exp\left[-\frac{\mathcal{H}}{D}\left(1-e^{-\beta D}\right)\right] , \tag{3}$$

where the ground state energy $\mathcal{H}_{g.s.}$ is subtracted from the energy expectation value, $\mathcal{H}$. It is an improved β expansion with the desired asymptotic behavior; $\mathcal{W}(\boldsymbol{Z})$ converges to a finite value less than one in the low temperature limit, $\beta \to \infty$, and reduces to a normal β expansion, $\exp(-\beta\mathcal{H}+\beta^2\sigma_E^2/2+\cdots)$, at high temperatures. This harmonic approximation is equivalent to assuming that the energy eigen component distribution within a wave packet is of Poisson type with the level spacing $D(\boldsymbol{Z})$, and it becomes exact for distinguishable particles in an external harmonic oscillator potential.

We have applied this harmonic approximation to the Antisymmetrized Molecular Dynamics(AMD) [4] wave function. In AMD, the energy dispersion can be estimated by using the imaginary time (or β) evolution of the wave packet parameters,

$$\sigma_E^2(\boldsymbol{Z}) = -\frac{d}{d\beta}\mathcal{H}_\beta(\boldsymbol{Z})\bigg|_{\beta=0} = \frac{\partial\mathcal{H}}{\partial\boldsymbol{Z}}\cdot\boldsymbol{C}^{-1}\cdot\frac{\partial\mathcal{H}}{\partial\bar{\boldsymbol{Z}}} , \quad \boldsymbol{C}\cdot\frac{d\boldsymbol{Z}_{\beta/2}}{d\beta} = -\frac{1}{2}\frac{\partial\mathcal{H}}{\partial\bar{\boldsymbol{Z}}} , \tag{4}$$

where the equation of motion for the normal time evolution is given by $i\hbar\boldsymbol{C}\cdot\dot{\boldsymbol{Z}} = \partial\mathcal{H}/\partial\bar{\boldsymbol{Z}}$. By using the energy expectation value and this energy dispersion, we have carried out the Monte Carlo integral (2) of $\mathcal{H}_\beta$ with the statistical weight $\mathcal{W}_\beta$ of Eq. (3).

In Fig. 1, we show the energy-temperature relation — so-called the caloric curve — of 40 nucleons confined in a sphere. Unfortunately, we could not see the energy gap, probably because the system is too small ($A = 40$) and the volume is fixed. However, it is clear that the temperature initially grows as $T \propto \sqrt{E}$ which is a typical behavior of the Fermi gas or liquid phase, and it converges to a classical line $T = 2E/3A + \text{constant}$ at high temperatures.

Compared to the classical results, in which the excitation energy is a linear function of temperature even at low temperatures, the excitation energy is strongly suppressed by incorporating quantum fluctuations. This suppression

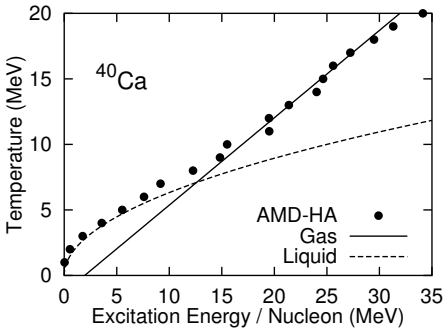

Figure 1: Caloric curve of ^{40}Ca [2]. The mean excitation energy per nucleon E^*/A for a canonical ensemble of 40 nucleons (20 protons and 20 neutrons) confined in a sphere with a radius 2.0 $A^{1/3}$ fm as a function of the temperature T. Circles show the calculated results with the harmonic approximation based on the AMD model. Solid and dashed lines show the temperature in gas and liquid phase.

comes from the intrinsic distortion effects. The energy expectation value of the distorted state, whose weighted average becomes the mean excitation energy, is calculated under the harmonic approximation to be,

$$\mathcal{H}_\beta(\boldsymbol{Z}) \equiv \frac{\langle \boldsymbol{Z}_{\beta/2}|\hat{H}|\boldsymbol{Z}_{\beta/2}\rangle}{\langle \boldsymbol{Z}_{\beta/2}|\boldsymbol{Z}_{\beta/2}\rangle} = -\frac{\partial}{\partial\beta}\log \mathcal{W}_\beta(\boldsymbol{Z}) = \mathcal{H}(\boldsymbol{Z})\ e^{-\beta D}\ . \tag{5}$$

The factor $e^{-\beta D}$ helps to reduce energy keeping the partition function finite.

3 Fragmentation at Fixed Temperature

Once the equilibrium distribution is given, we can construct a model which dynamically produces the desired equilibrium distribution $\mathcal{W}_\beta(\boldsymbol{Z})$ at equilibrium. For example, we can adopt a Fokker-Planck type equation or its equivalent Langevin equation,

$$\frac{Dq_i}{Dt} \ = \ V_i \ + \ \sum_j g_{ij}\zeta_j \ , \quad V_i = -\sum_j M_{ij}\,\frac{\partial \log(\mathcal{W}_\beta(\boldsymbol{Z}))}{\partial q_j} \ , \tag{6}$$

where $\{q_i\}$ are canonical variables satisfying $d\Gamma = \prod_i dq_i$, $\boldsymbol{M} = \boldsymbol{g}\cdot\boldsymbol{g}$ represents the mobility tensor, and ζ is the white noise, $\prec \zeta_i(t)\,\zeta_j(t') \succ = 2\delta_{ij}\,\delta(t - t')$. Although the stochastic term appearing here is somewhat similar to the usual Brownian force, the present random force contains fluctuations that come from the energy dispersion of each wave packet and thus has a quantal origin. Therefore, we refer to this random force as the *Quantal Langevin* force [2].

In the harmonic approximation (3), the Quantal Langevin equation for the phase space variables, $\{q_i\} = \{\boldsymbol{r}, \boldsymbol{p}\}$, can now be written as,

$$\dot{\boldsymbol{p}} = \boldsymbol{f} - \alpha\beta \boldsymbol{M}^p \cdot (\boldsymbol{v} - \boldsymbol{u}) - \beta \boldsymbol{M}^p \cdot \boldsymbol{u} + \boldsymbol{g}^p \cdot \boldsymbol{\zeta}^p \ , \tag{7}$$

$$\dot{\boldsymbol{r}} = \boldsymbol{v} + \alpha\beta \boldsymbol{M}^r \cdot \boldsymbol{f} + \boldsymbol{g}^r \cdot \boldsymbol{\xi}^r \ , \tag{8}$$

$$\boldsymbol{f} \equiv -\frac{\partial \mathcal{H}}{\partial \boldsymbol{r}} \ , \quad \boldsymbol{v} \equiv \frac{\partial \mathcal{H}}{\partial \boldsymbol{p}} \ , \quad \alpha = \frac{1 - \exp(-\beta D)}{\beta D} \leq 1 \ . \tag{9}$$

We have subtracted the energy dispersion related to the spurious zero-point center-of-mass motion of clusters in Eq. (7), by considering the relative velocity of each particle relative to the local collective motion with the velocity $\boldsymbol{u}$, which is close to the fragment CM motion [5]. The additional factor $\alpha \leq 1$ shows the modification of the classical fluctuation-dissipation theorem (Einstein relation). Since the diffusion term becomes relatively stronger than the drift term, the Quantal Langevin force generates more fluctuations in the space of $\{q_i\}$. When the energy dispersion of a wave packet is sufficiently small, α becomes close to unity. This is the classical limit where the normal Einstein relation is recovered.

In Fig. 2, we show the calculated nuclear fragment distributions at given temperatures. We put 40 nucleons in a box with the periodic boundary condition, and the quantal ($\alpha < 1$) or classical ($\alpha = 1$) Langevin force is included in the QMD model. In the quantum treatment, the intrinsic distortion is taken into account by solving the β evolution. It is clear that, in the Quantal Langevin treatment, more fragments are formed than in the classical case, and the results of the fragment grandcanonical model are well reproduced. This behavior is a result of the combined effects of the modified Einstein relation and the intrinsic distortion; while the former gives more fluctuations to nucleons and thus gives more excitation energies to fragments, the latter reduces fragment excitations. In a mechanically stable region, this combined effect can be expressed as the shift of effective classical temperature to the distorted states,

$$T'_{\rm eff} = \frac{g^2 e^{-D/T}}{\alpha\beta M} = \frac{D}{e^{D/T} - 1} < T \ . \tag{10}$$

This effective temperature is extracted by applying the Einstein relation to the Langevin equation of the distorted momentum [6], and the Quantal Langevin results at T well coincides with the classical Langevin results at $T'_{\rm eff}$. However, at around the critical temperature, the distortion enhances the small fluctuations generated by the Quantal Langevin force and thus causes cluster rearrangements. Therefore, for the fragmentation processes through the phase transition, shifting the effective temperature in a classical treatment is not capable to describe the above combined quantal effects. This is the mechanism of multifragmentation suggested by the Quantal Langevin model.

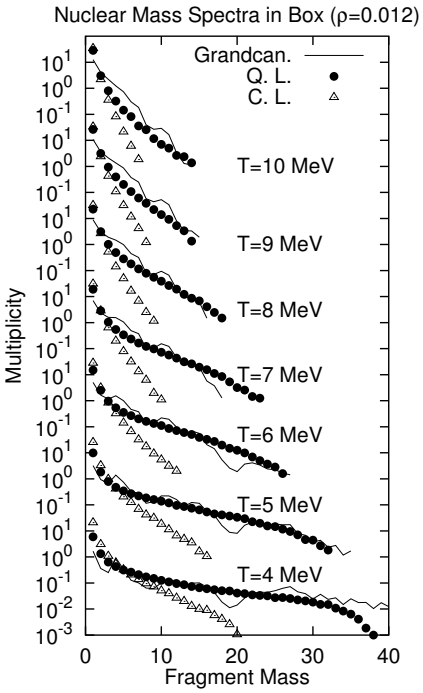

Figure 2: Thermal fragmentation [5]. Nuclear fragment mass distribution at given temperagures in a box with the periodic boundary condition. Solid circles and open triangles show the results of the simulation with the quantal and classical Langevin force, respectively. In the figure, the grandcanonical fragment population is also shown (solid line).

4 Multifragment Formation from Heavy-Ion Collision

We can now apply the Quantal Langevin model to the nucleus-nucleus collision, where the energy is given. In this case, the equilibrium distribution should be microcanonical, and the statistical weight is given by $\rho_{_E}(\boldsymbol{Z}) \equiv \langle \boldsymbol{Z}|\delta(E-\hat{H})|\boldsymbol{Z}\rangle$. The hamonic approximation described in Sec. 2 is equivalent to assuming that each wave packet has a (discrete) Poisson energy distribution. In nucleus-nucleus collisions, the total energy is much larger than the effective level spacing $D(\boldsymbol{Z})$ and we may then adopt a continuous Poisson distribution,

$$\rho_{_E}(\boldsymbol{Z}) \approx \frac{(\mathcal{H}/D)^{E/D}}{\Gamma(E/D+1)} \exp(-\mathcal{H}/D) \ . \tag{11}$$

Since this statistical weight has finite value even for those states with $\mathcal{H} \neq E$, the energy expectation value $\mathcal{H}$ can fluctuate around the given energy E. The drift coefficient can then be readily calculated,

$$V_i \simeq -\beta_{\mathcal{H}} \sum_j M_{ij} \frac{\partial \mathcal{H}}{\partial q_j} , \quad \beta_{\mathcal{H}} \equiv \frac{\partial \log(\rho_E)}{\partial \mathcal{H}} = \frac{\mathcal{H} - E}{\sigma_E^2} . \tag{12}$$

It is interesting to note that the drift term acts to restore the energy expectation value to a given one: when the Hamiltonian $\mathcal{H}$ is greater than the given energy E, the drift term reduces it, and vice versa. Furthermore, since the phase volume is larger for larger $\mathcal{H}$, the dynamical trajectory usually goes through the region $\mathcal{H} > E$. Therefore, fragments are cooled down in the final stage of collision, without emitting nucleons. In other words, although the wave packet wave functions with various expectation energies can contribute in the interacting region, they are projected onto their eigen energy component in the asymptotic region.

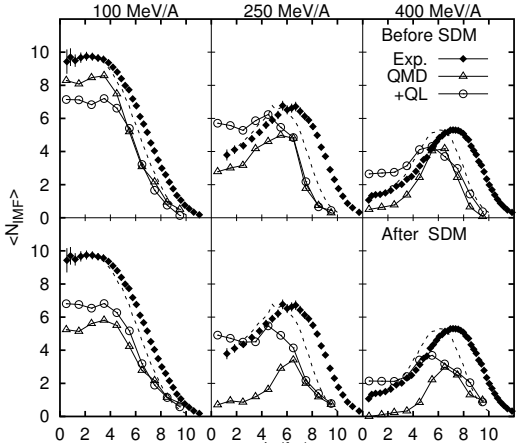

Figure 3: IMF ($3 \leq Z \leq 30$) Multiplicities in Au+Au collisions [5]. Circles and triangles indicate QMD results at given energies with and without the Quantal Langevin force, respectively. The upper and lower parts show the distributions before and after the statistical decay (SDM) calculation, respectively. The experimental data [7] are shown by solid diamonds. Dotted lines show the experimental data using a scaled impact parameter assuming a maximum impact parameter of 10 fm. The detector efficiency is not taken into account in the calculation.

We have incorporated this Quantal Langevin force at a given energy into the QMD model, and applied it to the multifragment formation in Au+Au collision. In Fig. 3, we show the calculated impact parameter dependence

of intermediate-mass fragment (IMF) average mulitplicities in ^{197}Au+^{197}Au collision in comparison with the experimental data by Tsang et al. [7]. We see that the treatments with and without the quantal Langevin force agree with each other qualitatively in the dyamical stage (upper part). For example, the IMF multiplicity has the peak at central collisions at $E/A = 100$ MeV, while the peak moves to finite impact parameter at higher incident energies. However, in the case of QMD without quantal Langevin force, the excitation energies of the primary fragments are large enough to largely eliminate the IMF component from the final mass distribution in the statistical decay stage. This tendency is more clear for central collisions, where the fragments are likely to be highly excited. On the other hand, QMD with the quantal Langevin force reduces the excitation energies of the primary fragments because of the quantum-statistical nature of the intrinsic degrees of freedom. As a result, the difference between the average multiplicities before and after the statistical decay is less than one in the quantal Langevin model.

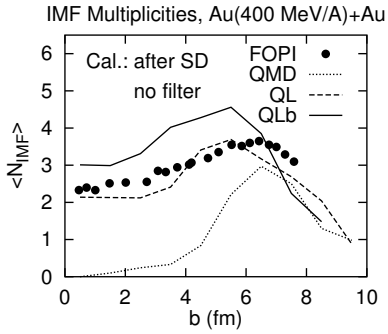

Figure 4: IMF ($3 \leq Z \leq 15$) Multiplicities in Au+Au collisions at 400 MeV/A. Dotted, dashed, and solid lines show the calculated impact parameter dependences of IMF multiplicities by using QMD, QMD with Quantal Langevin force (QL), and QL including cluster-cluster scattering, respectively. Statistical decay after dynamical stage is included in the calculation, and no filter is included. The experimental data [8] are shown by filled circles.

Recently, FOPI group have analyzed the clusterization from Au+Au collision in more detail, including charge and isotope distribution [8]. In Figs. 4 and 5, we compare the model calculation and their data. Including the quantum fluctuation effects (QL) cleary improves the description of fragment formation. However, it still underestimates light fragment yields. This may be because the two nucleon collision term, which is included in a classical way, somewhat spoils the quantal nature generated by the Quantal Langevin force. In order to avoid this defect partly, we have included scattering of $0s$-clusters at low nucleon densities (QLb). Namely, when a well defined $0s$-cluster $(d, t, ^3\mathrm{He}, \alpha)$

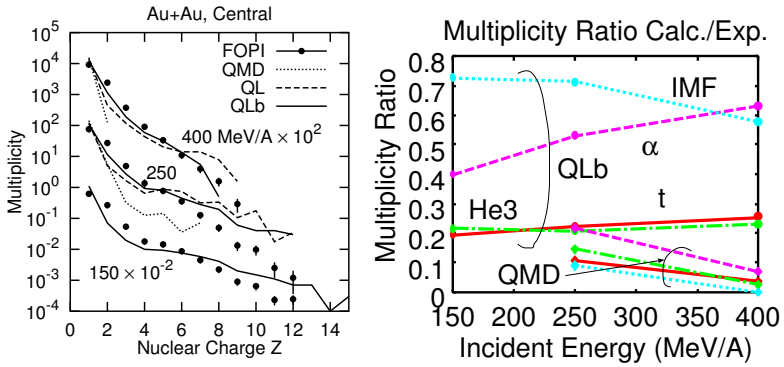

Figure 5: Left: Fragment charge distribution from central Au+Au collisions. Dotted, dashed, and solid lines show the calculated results with QMD, QL, and QLb, respectively (see text). Experimental data[8] are shown by filled circles. Circles and triangles indicate QMD results at given energies Right: Multiplicity ratio of the calculated results to the experimental data[8].

collides with other nucleons or 0s-clusters at nuclear surface, they are made to scatter elastically with the probability of a half even at high colliding energies of these clusters (shadow scattering). This cluster-cluster scattering enhances light charged fragment yields (Fig. 5, Left). In addition, IMF mulitplicities are increased, probably because these light charged particles can coalesce to make IMF.

5 Summary and Outlook

We have shown the basic idea and some applications of the Quantal Langevin model. The characteristic features of the Quantal Langevin model are the *larger fluctuations* and the *intrinsic distortion* of wave packets. The combination of these two features enhances fragments with low excitation. The inclusion of the quantal fluctuations has led to improved results for the nuclear caloric curve, the nuclear fragment mass distribution in a thermal environment, and the fragment multiplicities in Au+Au collisions.

Some problems still remain in the formulation and application of the Quantal Langevin model. First, the mobility tensor $\boldsymbol{M}$ cannot be determined by statistical requirements alone and it may be necessary to invoke other fluctuation schemes as well [9,10]. Second, it may be necessary to treat the energy dispersion related to the fragment center-of-mass motion more carefully. Finally, when antisymmetrization is imposed, the parameters of the wave packets are not canonical. Then the derivation of the dynamical equation requires the transformation matrix between the parameters and the canonical variables.

Finally, we have shown some preliminary results with cluster-cluster scattering. We expect that this procedure partly helps to avoid the defects of classical two-nucleon collision term. As a result, the calculated fragment yields becomes much closer to the experimental data. However, as can be seen in Fig. 5 (right), $A = 3$ fragment yield is still underestimated by a factor around four. Therefore, cluster-cluster rearrangement in nuclei or explicit treatment of coalescence may be necessary, since these processes are expected to occur in a short time and might not be expressed in terms of random force.

Acknowledgments

This work was supported in part by the Grant-in-Aid for Scientific Research (Nos. 07640365 and 09640329) from the Ministry of Education, Science and Culture, Japan, and by the Director, Office of Energy Research, Office of High Energy and Nuclear Physics, Nuclear Physics Division of the U.S. Department of Energy under Contract No. DE-AC03-76SF00098.

References

1. J. Pochadzalla et al., *Phys. Rev. Lett.* **75**, 1040 (1995);
   G. Raciti, in this proceedings.
2. A. Ohnishi and J. Randrup, *Phys. Rev. Lett.* **75**, 596 (1995); *Ann. Phys. (N.Y.)* **253**, 279 (1997).
3. A. Ohnishi and J. Randrup, *Nucl. Phys.* **A565**, 474 (1993).
4. A. Ono, H. Horiuchi, T. Maruyama, and A. Ohnishi, *Phys. Rev. Lett.* **68**, 2898 (1992); *Prog. Theor. Phys.* **87**, 1185 (1992).
5. A. Ohnishi and J. Randrup, *Phys. Lett.* **B394**, 260 (1997).
6. A. Ohnishi and J. Randrup, *Phys. Rev.* **A55**, 3315R (1997).
7. M.B. Tsang et al., *Phys. Rev. Lett.* **71**, 1502 (1993).
8. W. Reisdorf et al., *Nucl. Phys.* **A612**, 493 (1997).
9. A. Ono and H. Horiuchi, *Phys. Rev.* **C53** , 2958 (1996) .
10. F. Chapelle, G.F. Burgio, Ph. Chomaz, and J. Randrup, *Nucl. Phys.* **A540** , 227 (1992) .